Experimental study on pressure-velocity relation of near-field tip vortex using tomographic PIV

Hang Zhao[1], Wenxuan She[1], Qi Gao[1,*], Xueming Shao[1]

1: School of Aeronautics and Astronautics, Zhejiang University, China
*Corresponding author: qigao@zju.edu.cn

Keywords: Elliptical hydrofoil, tip vortex, pressure-velocity relation, TPIV.

ABSTRACT

The non-cavitating tip vortex in the near field of an elliptical hydrofoil is studied using tomographic particle image velocimetry (TPIV). By investigating the distributions of the axial velocity difference and streamwise vorticity, the formation and development of the near-field tip vortex are clearly revealed. In the near field, the axial flow within the tip vortex manifests a jet-like profile, and the majority of the vorticity is contained within the vortex core. A special position is identified during the streamwise evolution of the tip vortex, where the vortex core circulation reaches its local maximum for the first time and tip vortex cavitation (TVC) might be more prone to incept. In the vicinity of this crucial position, a concise relation between the static pressure along the tip vortex center line and the local velocity is derived by combining the three-dimensional measured velocity fields with the governing equations. Based on the Reynolds-averaged Navier-Stokes equation, it is revealed that the mean static pressure along the vortex center line is directly related to the local mean axial velocity, whereas the local velocity fluctuation has little impact on the mean static pressure. It is the first attempt to combine the three-dimensional measurement with the governing equations to investigate the near-field tip vortex flow, which might provide valuable insights for understanding and predicting tip vortex cavitation inception.

1. Introduction

Owing to the low static pressure in vortices, the cavitation is more likely to be induced, resulting in several adverse effects (R. E. Arndt, 1981). The cavitation induced by the tip vortices is known as the tip vortex cavitation (TVC), which appears earliest among all types of cavitation (Zhang et al., 2015) and has been found to be closely associated with the flow properties of the tip vortex (R. E. Arndt, 2002). It is important to investigate the tip vortex flow in details for revealing the underlying mechanism of vortex-induced cavitation. As early as 1962, McCormick Jr (1962) conducted a comprehensive study on cavitation produced by a trailing vortex. Particular attention was paid to the minimum pressure coefficient in the vortex (namely the static pressure at the vortex center), which can be used to estimate the critical cavitation number in vortical flow. Under the boundary-layer-type approximation, the pressure at the center of vortex can be derived by integrating the simplified Navier-Stokes equations in cylindrical coordinates (Batchelor, 1964; R. Arndt et al., 1991). In addition, the minimum pressure coefficient within the tip vortex can be estimated applying simple vortex models, which enable the characterization of the vortex based on its circulation and viscous core size (Boulon et al., 1999; Franc & Michel, 2006). However, it is still less intuitive for the evaluation of pressure in the vortical flow, and corresponding pressure-velocity relation has not been established.

In the current work, tomographic particle image velocimetry measurement is applied to the tip vortex in the near field of an elliptical hydrofoil. The three-dimensional tip vortex is illustrated in detailed. The pressure-velocity relation along the tip vortex center line is investigated by combining the three-dimensional measured velocity fields with the governing equations.

2. Materials and methods

Experiments were conducted in the high-speed cavitation tunnel of Zhejiang University, China. The dimensions of the test section are 1000 mm (length) $\times$ 200 mm (width) $\times$ 200 mm (height). The test model is an elliptical hydrofoil with a NACA $66_2 - 415$ cross section for producing the tip vortex. Its root chord c is 83.66 mm, and the half-span length b is 100 mm. The incident angle of the hydrofoil α is 10°. The Reynolds number Re_c defined based on the root-chord length c is 3.31×10^5, and corresponding free-stream velocity U_∞ is 4.0 m/s. The non-cavitating tip vortex flow was measured by a four-camera TPIV system, and the size of measurement volume is 35 mm $\times$ 20 mm $\times$ 18 mm with a magnification of 0.043 mm per voxel.

3. Results and discussion

3.1. Mean flow field

Figure 1a gives the distributions of time-averaged dimensionless axial velocity difference ($u_d = u - U_\infty$) in the planes $x/c = 0, 0.08, 0.16, 0.24$. Around $x/c = 0$, the tip vortex is at the early growth stage, and an axial velocity deficit ($u_d/U_\infty = -0.1 \sim -0.15$) is clearly displayed in the vortex core. That is to say, the axial flow of the tip vortex initially exhibits a wake-like profile. It can be observed that this velocity deficit appears to originate from the boundary layers on the suction side of the hydrofoil. As the tip vortex develops downstream, the in-core axial flow is accelerated, and its velocity is close to U_∞ at $x/c = 0.08$. For further downstream, a velocity excess ($u_d/U_\infty \approx 0.1$) is presented in the vortex core, and the in-core axial flow exhibits a jet-like profile. The distributions of the dimensionless streamwise vorticity are presented by figure 1b. At $x/c = 0$, the tip vortex is attached to the suction side of the hydrofoil, and the in-core vorticity is at a rather low level. As the tip vortex progresses downstream, the in-core vorticity continuously increases. For $x/c \geq 0.16$, the tip vortex has started to leave the trailing edge and enter the wake region, and the in-core vorticity has reached to a quite high level with no sign of decay. In the whole near filed, the majority of the streamwise vorticity is mainly concentrated within the tip vortex core.

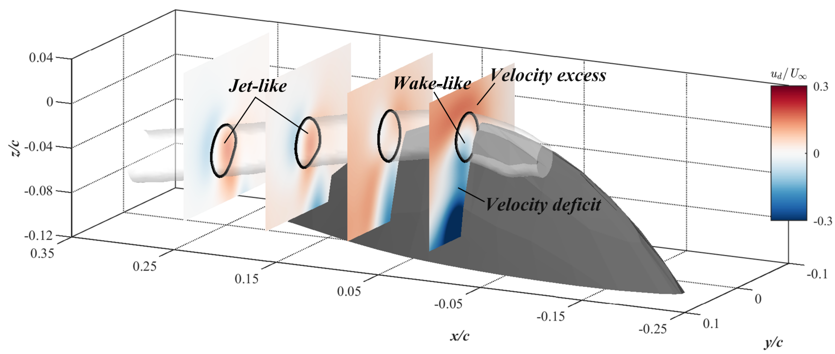

(a)

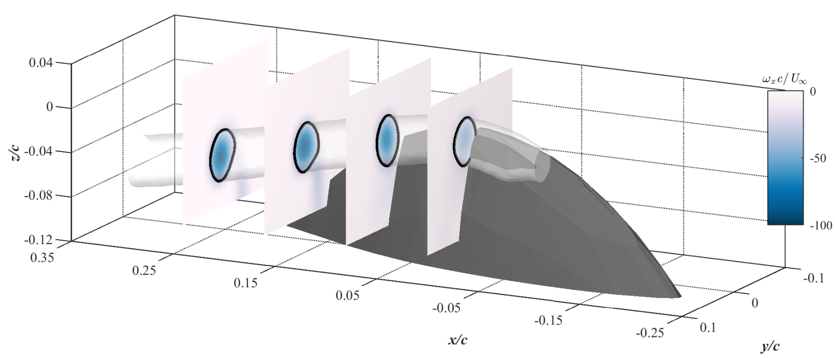

(b)

Figure 1. Time-averaged (*a*) axial velocity difference and (*b*) streamwise vorticity distributions in the planes $x/c = 0, 0.08, 0.16, 0.24$.

The streamwise evolution of the dimensionless core circulation Γ_x^* is presented in figure 2. Two distinct stages of the circulation evolution are clearly observed. Γ_x^* grows rapidly at first and then is maintained at a relatively constant level with the tip vortex propagating further downstream. The streamwise position where Γ_x^* firstly reaches the plateau is at about $x/c = 0.16$ (Zhao et al., 2023). Dreyer et al. (2014) provided a general estimation formula of the vortex center pressure that the vortex center pressure is negatively correlated with the vortex circulation. Combined with figure 2, the pressure along the vortex center line firstly drops to its minimum at $x/c = 0.16$ where Γ_x^* reaches its local maximum, and the tip vortex cavitation might be more prone to incept at this position. In the current work, the mean static pressure at the tip vortex center can be obtained from this general estimation formula and the Rankine vortex model (Saffman, 1995), which can be used to further calculate the pressure gradient along the vortex center line.

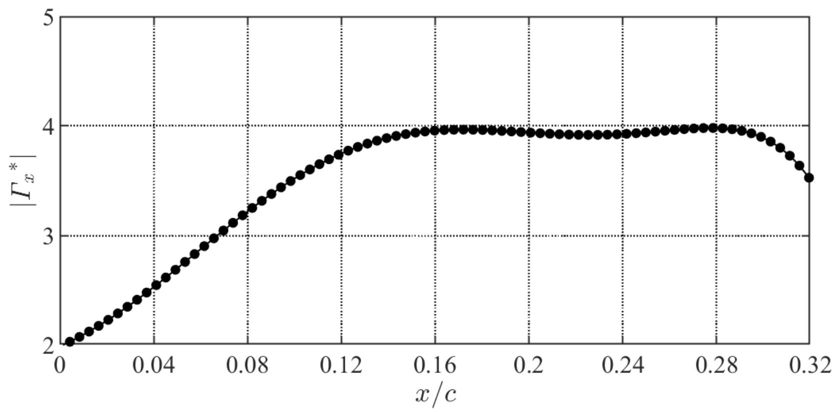

Figure 2. Streamwise evolution of dimensionless core circulation.

3.2. Pressure-velocity relation

As the vortex line is basically aligned with the free-stream, the tip vortex can be considered as quasi-streamwise. In other words, the variation of pressure and velocities along the vortex center line can be approximated as corresponding variation along the streamwise direction. Moreover, since the non-cavitating tip vortex stably exists in the near wake region, the corresponding flow field is in a quasi-steady state, namely $\dfrac{\partial}{\partial t} = 0$. Thus, the $x-$component of the reordered dimensionless Reynolds-averaged Navier-Stokes (RANS) equation can be obtained

$$\underbrace{\frac{\partial \overline{p}^*}{\partial x_1^*}}_{p_x^*} = \underbrace{-\overline{u}_j^*\frac{\partial \overline{u}_1^*}{\partial x_j^*}}_{C_x^*} + \underbrace{\frac{1}{Re}\frac{\partial^2 \overline{u}_1^*}{\partial x_j^* \partial x_j^*}}_{\epsilon_x^*} + \underbrace{\frac{\partial(-\overline{u_1'^* u_j'^*})}{\partial x_j^*}}_{R_x^*} \,. \tag{1}$$

Considering Eq.(1) along the vortex center line, the individual effects of convective (C_x^*), viscous (ϵ_x^*) and Reynolds-stress (R_x^*) terms on the streamwise gradient of mean pressure (p_x^*) are studied in the vicinity of $\varGamma_x^*$ firstly reaching its local maximum ($x/c = 0.13 \sim 0.21$).

Terms in Eq.(1) are presented in figure 3a. The pressure gradient term is basically consistent with the sum of other terms in both magnitude and development trend, and the residual between the two sides of governing equation is at a relatively acceptable level. The experimental data satisfies the constraints of the Reynolds-averaged N-S equation.

Each dimensionless term on the right-hand side of Eq.(1) is plotted as a function of x/c in figure 3b. The viscous term ϵ_x^* approximates zero, indicating that the viscous effects on the mean pressure gradient is negligible. The Reynolds-stress term R_x^*, which is directly related to the fluctuating velocity, also has a rather limited impact on the mean pressure gradient. The right-hand side of Eq.(1) is dominated by the convective term C_x^*. As shown by figure 3c, C_x^* can be further divided into three sub-terms, of which $-\overline{u^*}\dfrac{\partial \overline{u^*}}{\partial x^*}$ plays a vital role, especially around $x/c = 0.16$.

Although $-\overline{v^*}\dfrac{\partial \overline{u^*}}{\partial y^*}$ and $-\overline{w^*}\dfrac{\partial \overline{u^*}}{\partial z^*}$ can not be neglected, they are comparable in magnitude and opposite on sign. Consequently, the overall effect of the convective term C_x^* on the mean pressure gradient p_x^* is primarily determined by the streamwise convection $-\overline{u^*}\dfrac{\partial \overline{u^*}}{\partial x^*}$, making it dominant in the production of p_x^*.

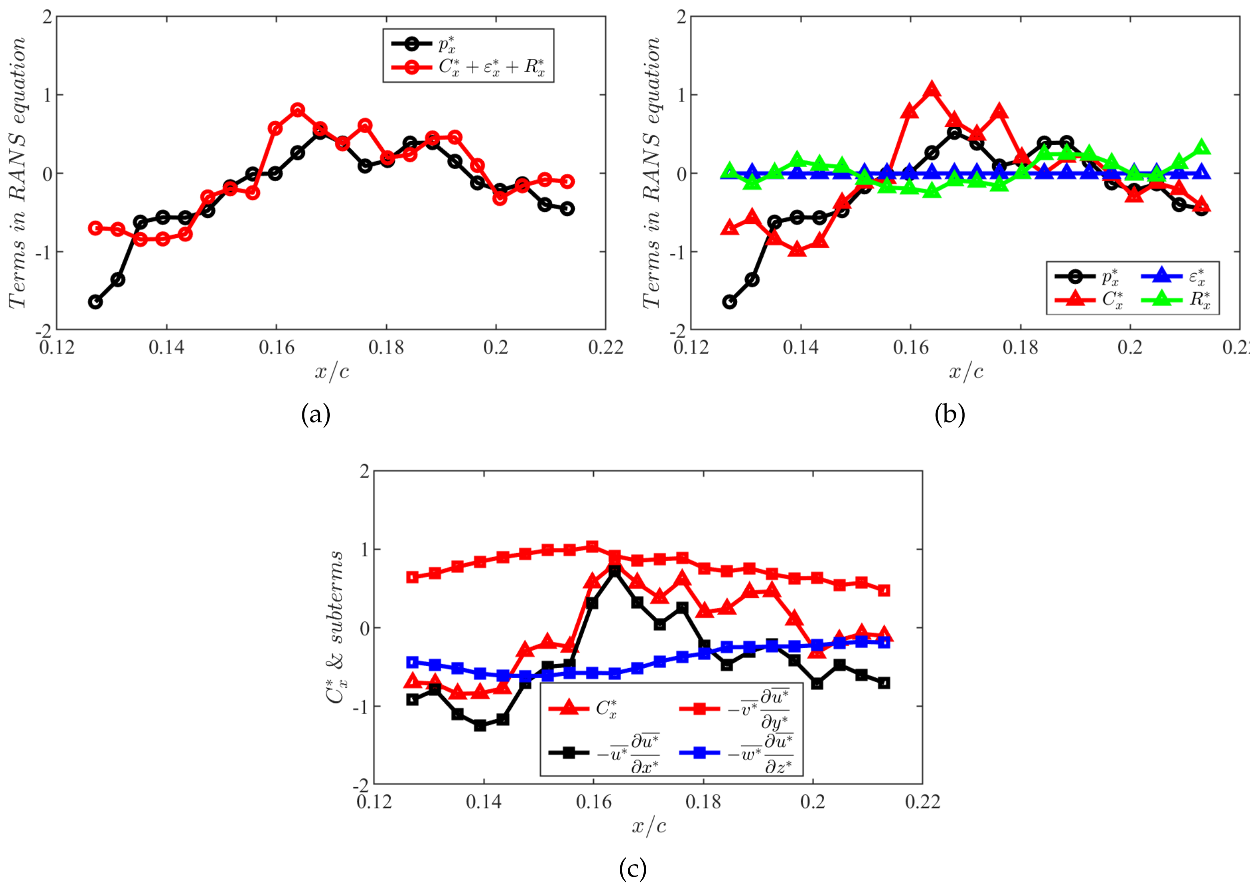

Figure 3. (*a*) Comparison between the mean pressure gradient term p_x^* and the sum of other terms on the ride-hand side of Eq.(1); (*b*) comparison between the mean pressure gradient term p_x^* and each term on the ride-hand side of Eq.(1); (*c*) sub-terms of the convective term C_x^*.

For the pressure-velocity relation in RANS equations, it is obtained that the streamwise pressure gradient is mainly relevant to the corresponding convection, i.e., $\dfrac{\partial \overline{p}}{\partial x} \sim -\rho\overline{u}\dfrac{\partial \overline{u}}{\partial x}$. Further integrating gives a scaling that $\overline{p} \sim -\dfrac{1}{2}\rho\overline{u}^2$. Interestingly, this relation is quite similar to the Bernoulli's principle (the simplified form with the gravitational potential energy ignored). Consequently, it can be concluded that the mean static pressure along the tip vortex center line is most closely correlated with the local mean axial velocity, whereas the fluctuating velocities have little impact on the local mean pressure (recall that the Reynolds-stress term R_x^* is quite small in figure 3b). The mean axial velocity can thus be employed to estimate the static pressure distribution along the vortex center line, providing a rough prediction of the position of TVC inception. It implies that the static pressure at the vortex center might be quite low for the tip vortex with jet-like axial flow (the axial velocity in the vortex is higher than the free-stream velocity), as shown in figure 1a. In other words, this kind of tip vortex is more prone to induce cavitation. Furthermore, this pressure-velocity relation also provides a theoretical explanation for some experimental observations, such as the mitigation of tip vortex cavitation by reducing axial velocity (Lee et al., 2018; Amini et al., 2019) and the positive correlation between vortex circulation and axial velocity (Anderson & Lawton, 2003).

4. Conclusions

The present study focuses on the near-field tip vortex flow. The pressure-velocity relation is studied based on the $x-$component of the Reynolds-averaged Navier-Stokes equation. In the vicinity of the vortex core circulation firstly reaching its local maximum, it is derived that the mean static pressure at the vortex center is directly related to the local mean axial velocity, while the local velocity fluctuation has little impact on it. This investigation of the pressure-velocity relation would provide valuable insights into understanding and predicting tip vortex cavitation inception.

Acknowledgments

This work was supported by the National Key Research and Development Program of China (Grant No. 2020YFA0405700).

References

Amini, A., Reclari, M., Sano, T., Iino, M., & Farhat, M. (2019). Suppressing tip vortex cavitation by winglets. *Experiments in Fluids*, *60*(11), 1–15. doi: 10.1007/s00348-019-2809-z

Anderson, E. A., & Lawton, T. A. (2003). Correlation between vortex strength and axial velocity in a trailing vortex. *Journal of Aircraft*, *40*(4), 699–704. doi: 10.2514/2.3148

Arndt, R., Arakeri, V., & Higuchi, H. (1991). Some observations of tip-vortex cavitation. *Journal of Fluid Mechanics*, *229*, 269–289. doi: 10.1017/S0022112091003026

Arndt, R. E. (1981). Cavitation in fluid machinery and hydraulic structures. *Annual Review of Fluid Mechanics*, *13*(1), 273–326. doi: 10.1146/annurev.fl.13.010181.001421

Arndt, R. E. (2002). Cavitation in vortical flows. *Annual Review of Fluid Mechanics*, *34*(1), 143–175. doi: 10.1146/annurev.fluid.34.082301.114957

Batchelor, G. (1964). Axial flow in trailing line vortices. *Journal of Fluid Mechanics*, *20*(4), 645–658. doi: 10.1017/S0022112064001446

Boulon, O., Callenaere, M., Franc, J.-P., & Michel, J.-M. (1999). An experimental insight into the effect of confinement on tip vortex cavitation of an elliptical hydrofoil. *Journal of Fluid Mechanics*, *390*, 1–23. doi: 10.1017/S002211209900525X

Dreyer, M., Decaix, J., Münch-Alligné, C., & Farhat, M. (2014). Mind the gap: a new insight into the tip leakage vortex using stereo-piv. *Experiments in Fluids*, *55*, 1–13. doi: 10.1007/s00348-014-1849-7

Franc, J.-P., & Michel, J.-M. (2006). *Fundamentals of cavitation* (Vol. 76). Springer science & Business media.

Lee, S.-J., Shin, J.-W., Arndt, R. E., & Suh, J.-C. (2018). Attenuation of the tip vortex flow using a flexible thread. *Experiments in Fluids*, *59*, 1–12. doi: 10.1007/s00348-017-2476-x

McCormick Jr, B. (1962). On cavitation produced by a vortex trailing from a lifting surface. *Journal of Basic Engineering*, *84*, 369–378. doi: 10.1115/1.3657328

Saffman, P. G. (1995). *Vortex dynamics*. Cambridge university press.

Zhang, L.-x., Zhang, N., Peng, X.-x., Wang, B.-l., & Shao, X.-m. (2015). A review of studies of mechanism and prediction of tip vortex cavitation inception. *Journal of Hydrodynamics*, *27*(4), 488–495. doi: 10.1016/S1001-6058(15)60508-X

Zhao, H., Tu, H., She, W., Gao, Q., Cao, Y., Peng, X., & Shao, X. (2023). An experimental study on near-field tip vortex of an elliptical hydrofoil using tomographic particle image velocimetry. *Exp. Fluids*, *64*, 195. doi: 10.1007/s00348-023-03735-3